Normal Vibrational Analysis of the Syndiotactic Polystyrene s(2/1)2 Helix

Normal Vibrational Analysis of the Syndiotactic Polystyrene s(2/1)2 Helix

F. Javier Torres, Bartolomeo Civalleri, Alessio Meyer* [(a)]

Pellegrino Musto[(b)]

Alexandra R. Albunia, Paola Rizzo, Gaetano Guerra* [(c)]

[(a)] Dipartimento di Chimica IFM and NIS Centre of Excellence, Università di Torino, Via Pietro Giuria 7, 10125 Torino, Italia

[(b)] Institute of Chemistry and Technology of Polymers (ICTP), National Research Council of Italy, via Campi Flegrei, 34, Olivetti Building, 80078 Pozzuoli (Napoli), Italia.

[(c)] Dipartimento di Chimica and INSTM Research Unit, Università di Salerno, Via Ponte don Melillo, 84084 Fisciano (SA), Italia

RECEIVED DATE

Abstract

The full vibrational spectra of γ, δ and ε crystalline phases of syndiotactic polystyrene (sPS), i.e. phases presenting the s(2/1)2 helical conformation, have been experimentally determined and compared with that calculated at the B3LYP/6-31G(d,p) level of theory for an infinite helix. The assignment of the different modes was highly facilitated and validated by the experimental evaluation of the direction of the transition moment vector of most IR peaks, which was for the first time made possible by measurements on s-PS films with different uniplanar orientations of the crystalline phase. The normal vibration analysis of most representative modes of the periodic model allowed us to give a general description of each one, which was further confirmed by the direct inspection of mode animations.

I. Introduction

Syndiotactic polystyrene (sPS) is a polymeric material with high melting point, high chemical stability and high crystallization rate, which has also received attention from the research community for its ability to form co-crystalline phases (clathrates[1-6] and intercalates[7-10]) with several low-molecular-mass molecules as well as two nanoporous crystalline phases (δ[11-14] and ε[15,16]), i.e. crystalline phases with empty space being available for sorption of suitable guest molecules.

Its complex polymorphic behavior,[17-20] making some simplifications, can be described in terms of two crystalline forms, α[21-23] and β,[24,25] containing planar zigzag chains and three forms, γ,[19,26,27] δ and ε, containing s(2/1)2 helical chains (helical repetition of two structural units in one turn, the structural unit being formed by two monomeric units). These helices are also present in all known s-PS co-crystalline phases[1-10] and are generated by TTGG conformational sequences.[28-30] A projection along the chain axis of a s(2/1)2 s-PS helix is shown in Figure 1.

Several Fourier Transform Infrared (FTIR) studies of the different crystalline phases of sPS have been reported in the literature.[31-44] These studies have clearly established characteristic absorption peaks of the trans-planar conformation as well as of the s(2/1)2 helical conformation. On the contrary, only a limited number of studies have appeared on the Raman spectroscopy of the various crystalline forms of sPS, and most of them are concerned with the *trans-planar* conformation.[45-48] A systematic analysis of the Raman spectra of the helical modifications appears therefore highly desirable in view of the optimum scattering capability of these crystalline forms, which produce high quality and essentially noise-free spectra. These can be used for quantitative purposes, and in particular, to develop methods for the evaluation of the crystallinity degree. Further advantages arise from the non-destructive character of the method and the possibility to perform measurements on samples in the form of powders or films of any thickness. Raman spectroscopy is to be regarded as a more versatile technique than FTIR, which can be usefully applied only to films few μm thick.

Although vibrational spectroscopy represents a powerful technique that allows the description of the sPS different crystalline forms, a complete normal mode analysis is essential to further understand the structural dynamics of the material and to clearly distinguish the conformationally sensitive modes. As for s-PS chains, such normal mode analysis has been deeply studied for the trans-planar conformation,[45,49] while only a preliminary and incomplete analysis has been reported for the helical s(2/1)2 conformation.[50]

In a recent preliminary note,[51] simulated spectra of an infinite chain model of a s(2/1)2 sPS helix (as obtained at the B3LYP/6-31G(d,p) by using the CRYSTAL06 code) have been compared with the FTIR spectrum of the δ form for the spectral range 1400-500 cm^{-1}. In that note, it was shown that the occurrence for s-PS of films with different uniplanar orientations of the crystalline phase[26,52-56] allows an experimental evaluation of the orientation of transition moment vectors (TMV) of vibrational modes corresponding to most infrared peaks. This information enormously facilitated the difficult task of assigning the observed peaks to vibrational modes of these complex polymer helices.[51]

In this paper, we extend our previous work by comparing vibrational frequencies, dipole moment directions and relative IR intensities of peaks of the ab-initio simulated spectrum of the s(2/1)2 sPS helix with experimental FTIR and RAMAN spectra of films presenting γ, δ and ε crystalline phases of s-PS, for the wavenumber range 4000-30 cm^{-1}. Here, the same strategy of a previous paper on the much more simple trans-planar chain is followed.[49] The purpose is to take advantage of both approaches, in particular of the ab-initio simulation, to obtain a full vibrational analysis of helical sPS. Moreover, graphical animations of all the normal modes have been used to confirm the results of the performed normal vibrational analysis by direct inspection of each mode.

II. Experimental and Computational Methods

A. Experimental Section.

a. Materials

Syndiotactic polystyrene pellets were supplied by Dow Chemical under the trademark Questra 101. ^{13}C nuclear magnetic resonance characterization showed that the content of syndiotactic polystyrene triads was over 98%. The weight-average molar mass obtained by gel permeation chromatography (GPC) in trichlorobenzene at 135°C was found to be $M_w=3.2x10^5$ with the dispersity index, $M_w/M_n=3.9$.

Powders have been obtained by milling of the s-PS pellets. δ form powders have been obtained by treatment with boiling THF, followed by immersion in acetonitrile for 90 min. γ form powders have been obtained by annealing of δ form powders at 150°C. ε form powders have been obtained by diffusion of $CHCl_3$ in γ form powders, followed by immersion in acetonitrile for 30 min.

Unoriented amorphous films 20-100 μm thick have been obtained by melt extrusion. γ form unoriented semicrystalline films have been obtained by acetone treatment of amorphous films followed by annealing at 150°C for 1 hour. δ and ε form films have been obtained by THF and $CHCl_3$ diffusion, respectively, in unoriented γ form films,[57] followed by guest removal effected by immersion in acetonitrile for 30 min.

δ form films with *a* and *c* crystalline axes preferentially parallel to the film plane (thereafter $a_{//}\,c_{//}$ uniplanar orientation)[26] and with the *a* and *c* axes perpendicular and parallel to the film plane (thereafter $a_{\perp}\,c_{//}$ uniplanar orientation)[55,56] have been obtained by guest removal from co-crystals with chloroform and 1,4-dimethylnaphthalene, respectively. These two co-crystalline films have been obtained by casting from 0.5 wt% solution[26] and by diffusion in unoriented amorphous film,[55]

respectively. By annealing of these films at 150°C for 1 hour, γ form films with ($a_{//}$ $c_{//}$) and ($a_{\perp}$ $c_{//}$) uniplanar orientations have been obtained, respectively.

Mesomorphic uniaxially oriented films[58-60] have been obtained by monoaxial stretching of amorphous extruded sPS films, at draw ratios λ = (final length/initial length) ≈ 3 and at constant deformation rate of 0.1 sec^{-1}, in the temperature range 105-110°C with a Brukner stretching machine. Uniaxial δ form semicrystalline films have been obtained by exposure for 3 days to CS_2 vapors of these uniaxially oriented films. Uniaxial γ form films have been obtained by annealing uniaxial δ form film at 150°C for 1 hour. Uniaxial ε form semicrystalline films have been obtained by diffusion of $CHCl_3$ in uniaxial γ form films and by subsequent guest removal by immersion in acetonitrile for 30 min.

b. Techniques

The different crystalline phases as well as their different kinds of orientation, which have obtained by the procedures described in the previous section, have been verified by Wide-Angle X-ray Diffraction (WAXD) patterns. WAXD patterns with nickel filtered CuKα radiation were obtained, in reflection, with an automatic Bruker diffractometer.[16,17] WAXD patterns were also obtained, in transmission, by using a cylindrical camera (radius = 57.3 mm). In the latter case the patterns were recorded on a BAS-MS imaging plate (FUJIFILM) and processed with a digital imaging reader (FUJIBAS 1800). In particular, to recognize the kind of crystalline phase orientation, photographic X-ray diffraction patterns were taken by having the X-ray beam parallel to the film surface and by placing the film sample parallel to the axis of the cylindrical camera.[26,53-56]

Infrared spectra were obtained at a resolution of 2.0 cm^{-1} with a Vector 22 Bruker spectrometer and/or with a Perkin Elmer System 2000 spectrometer. Both instruments were equipped with a

deuterated triglycine sulphate (DTGS) detector and a Ge/KBr beam splitter. The frequency scale was internally calibrated to 0.01 cm^{-1} using a He-Ne reference laser. 32 scans were signal averaged to reduce the noise. The thickness of films used for infrared measurements was always comprised between 20 and 40 μm, in order to keep the peaks of interest in the range of absorbance - concentration linearity.

Polarized infrared spectra were recorded by the use of a SPECAC 12500 wire grid polarizer. The degree of axial orientation relative to the crystalline phase has been formalized on a quantitative numerical basis using the Hermans' orientation function. In particular, the order parameter of the 571 cm^{-1} bands has been directly used as a measure of the axial orientation function (f_{cIR}, which is equal to unity for perfect alignment and null for random orientation)[58-60] for helical crystalline phases. For the used semicrystalline uniaxially stretched films f_{cIR} is equal to 0.94 (γ), 0.90 (δ) and 0.84 (ε).

The procedure of subtraction of the spectrum of the amorphous phase from the spectra of the semicrystalline samples, which has been used in Figure 2, has been described in detail in ref.39 and based on the use of the 1379 cm^{-1} peak, as suggested for helical crystalline phases of s-PS.[44]

The degree of crystallinity of the used unoriented γ and δ sPS films is 38% and 35%, respectively, as evaluated according to the IR procedure described in Refs. 39 and 44.

Raman spectra were collected on semicrystalline powder samples and amorphous films with a Nexus 670 FT-Raman spectrometer from Nicolet (Madison, WI) equipped with a CaF_2 beam splitter and an Indium-Gallium Arsenide (InGaAs) photoelectric detector. Collection was performed on the 180° backscattered radiation. The excitation source was a diode-pumped Nd-YAG laser (λ = 1064 nm) operating at a laser power of 750 mW. The spectra were collected in a Raman-shift range between 100 and 3700 cm^{-1} at a resolution of 4 cm^{-1}. Signal averaging over at list 500 consecutive scans was performed to improve the signal-to-noise ratio.

B. Computational Section.

The model, employed for the present study, was an infinite one-dimensional chain of the s(2/1)2 sPS, which was constructed by the application of the symmetry operators of the $P2_122$ rod group to its irreducible part and the repetition of the resulting unit in the chain axis direction.

Even if calculations could be performed on the crystalline structures of the s(2/1)2 sPS phases, the adopted level of theory does not include dispersive effects needed for a correct description of the crystal packing. Therefore, for consistency, we decided to concentrate on the isolated infinite chain model that includes all of the most relevant vibrational modes and describes γ, δ and ε phases of sPS.

The *ab-initio* quantum mechanical calculations were performed with the periodic CRYSTAL06 code.[61] The B3LYP Hamiltonian[62] together with an all-electron 6-31G(d,p) Gaussian-type basis set were used as level of theory. The DFT exchange-correlation contribution is evaluated by numerical integration over the cell volume[63]. Radial and angular points of the atomic grid are generated through Gauss-Legendre and Lebedev quadrature schemes. As discussed in Ref. [63], a pruned grid containing 75 radial points and a variable number of angular points, with a maximum of 974 on the Lebedev surface in the most accurate integration region, was used in the present study.

The atomic positions and the lattice constant were fully relaxed. Default optimization algorithms and convergence criteria were adopted.[61,64] Once the equilibrium geometry was determined, the normal frequencies at the Γ point were computed, within the harmonic approximation, by diagonalizing the mass-weighted Hessian matrix. CRYSTAL06 calculates analytically the potential energy first derivatives with respect to the atomic displacements from the equilibrium positions, whereas second derivatives are calculated numerically.[63,65] The energy tolerance for the SCF process was set to 10^{-10} Hartree. In order to compare the computed and the experimental spectra and for consistency with our previous work[51], the resulting computed frequencies were scaled by a factor of 0.972 to best fit the experimental values in the most relevant spectral range 1400-500 cm^{-1}.

The IR intensity A_i of the i-th mode is defined as follows:

$$A_i \propto d_i \left| \frac{\partial \mu}{\partial Q_i} \right|^2$$

It is proportional to the degeneracy d_i of the i-th mode that multiplies the square of the first derivative of the cell dipole moment with respect to the normal mode coordinate Q_i. The latter was computed numerically by using localized Wannier functions in the unit cell.[66,67] At present, Raman intensity calculation is still not available in the current release of the CRYSTAL06 code. TMV directions were derived from the Cartesian Born charge tensor by computing the angle formed with the x, y and z axes, respectively. Since the model chain is oriented along the z-axis and for symmetry reason, TMV directions were clearly identified without uncertainty.

III. Results and Discussion

A. Vibrational spectra of helical s-PS crystalline phases

Polarized FTIR spectra of γ, δ and ε crystalline forms of sPS are reported for the wavenumber range 3150-400 cm^{-1} in Figure 2. These spectra have been obtained by subtraction of the spectrum of a fully amorphous s-PS film from FTIR spectra of uniaxially oriented (for $\lambda \approx 3$) films including γ, δ and ε phases, by following the procedure described in refs. 39 and 44.

The spectra of Figure 2 clearly show that most absorbance peaks (nearly 70%) can be easily divided in two classes: those which are prominent in the spectra taken with polarization plane parallel (thin lines) or perpendicular (thick lines) to the draw direction (i.e., to the polymer chain axis). As discussed in detail in Ref. 51, the occurrence for s-PS of films with different uniplanar orientations of the crystalline phase allows, for most infrared peaks, an experimental evaluation of the orientation of transition moment vectors (TMV) also in the plane perpendicular to the chain axis. In particular, due to symmetry considerations, TMV have to be along the binary axes perpendicular to the helix, i.e. along the axes indicated by x and y in Figure 1. Peaks corresponding to vibrational modes parallel and perpendicular to the chain axis are indicated as z and ⊥ in Figure 2. For the other peaks, the attribution of the direction of the TMV is uncertain. As confirmed by the calculated spectra of the next section, this is due to the superposition of some of the 141 IR-active vibration modes of the s(2/1)2 s-PS helix.

Unpolarized FTIR spectra of semicrystalline s-PS films presenting γ and δ phases, with ($a_{//}\, c_{//}$) or ($a_{\perp}\, c_{//}$) orientations, are reported in Figure 3. On the basis of molecular symmetry considerations and of the knowledge of the crystalline structure of the δ-form,[11] for films presenting the ($a_{//}\, c_{//}$) orientation, "perpendicular" vibrational modes polarized along the x and y directions maximize and minimize their absorbances, respectively. On the other hand, for films presenting the ($a_{\perp}\, c_{//}$)

orientation, “perpendicular” vibrational modes polarized along the x and y directions present reduced and increased absorbances, respectively.

It is worth noting that this procedure allows the directions of TMV to be attributed for all s-PS peaks, which characterize the helical conformation, i.e. peaks being absent or of much lower intensity for amorphous and trans-planar chains.[31-44] In particular, the δ-form helical peaks located at 1320, 934, 780, 601, 548 and 503 cm^{-1} present TMV directions along the perpendicular binary axis which passes through the external methylenes (x in Figure 1) while the helical peak located at 608 cm^{-1} presents a TMV direction along the perpendicular binary axis which passes through the internal methylenes (y in Figure 1). A complete list of the experimentally evaluated TMV directions is presented in the fourth column of Table 3.

It is also worth noting that some of the vibrational peaks are packing sensitive since they present different positions for different crystalline forms. Particularly packing-sensitive are the peaks located at 909, 610, 599 and 539 cm^{-1} for the γ and ε forms and at 906, 608, 601 and 535 cm^{-1} for the δ-form[20] (Table 3, see also Figure 11 of Ref. 44). Moreover, the peak observed at 1379 cm^{-1} for fully amorphous films, is split at 1387–1376 cm^{-1} for γ and ε crystalline forms and at 1392–1378 cm^{-1} for the δ-form (inset of Figure 4 and Table 3).[44]

The Raman spectra of an amorphous s-PS film and a semicrystalline film in the δ form are compared in Figure 5, traces A and B, respectively. The development of crystallinity of the TTGG type induces well detectable changes in the spectrum as highlighted by the insets of Figure 5. In particular, the regions most sensitive to conformational order are located in the wavenumber ranges between 1520 and 1120 cm^{-1}, 960 and 720 cm^{-1} and between 690 and 130 cm^{-1}.

The presence of the helical crystalline phases is seen to transform the amorphous peak located at 1451 cm^{-1} with a shoulder at lower frequency into a well resolved doublet with maxima at 1451 and 1440 cm^{-1}. It is worth noting that, in the case of the *trans-planar* forms (α and β), crystal field

splitting was suggested for this peak on the basis of the IR results, while a negligible effect was found in the Raman spectra. The strong effect observed for the three crystalline phases of s-PS exhibiting *helical* chains (γ,δ and ε) is likely to be originated due to the helical conformation of the chains of the crystalline phase.

Preliminary results on samples of different crystallinity and/or containing different amounts of guest molecules indicate that the intensity ratio I_{1440}/I_{1451} changes quite substantially. On the basis of these considerations, it can be anticipated that the above ratio may be taken as a sensitive measure of the overall structural order present in the sample.

Other peaks absent in the spectrum of the amorphous sample and characteristic of the crystalline phase are detected at 1355, 1339, 1250, 843, 801, 758, 538, 442, 417, 241, 218 and 151 cm^{-1}. No detectable differences are observed between the Raman spectra of the three helical crystalline forms γ, δ and ε.

B. Calculated vibrational spectrum of the s(2/1)2 helix of s-PS

Before discussing the normal modes of the s(2/1)2 chain model, it is worth noting that the optimized structure is in good agreement with available experimental data for the δ crystalline form of s-PS. Indeed, the computed pitch of the helix is 7.8 Å in excellent agreement with the value of 7.7-7.9 Å for the *c*-axis of the crystalline structures of the *δ*,[11] ε[16] and co-crystalline[1-5] phases of s-PS. Also, internal coordinates such as bond angles and torsion angles are consistent with those assumed for the X-ray diffraction analyses.[11] The computed bond angle on the methine carbon atoms is 112°, while those on the methylene carbon atoms are 115° and 118°; torsion angles for the helix are 179° and 63°.

On the basis of the $P2_122$ rod group (whose factor group is isomorphous to D_2 point group) the computed frequencies were classified by symmetry, and according to the selection rules, their IR

and/or Raman activity was determined. The resulting symmetry classification, which is automatically performed by CRYSTAL06, is as follows:

$$\Gamma = 47A \oplus 47B_1 \oplus 47B_2 \oplus 47B_3$$

In this set, the three acoustic modes and the one associated with the rotation of the polymer about the periodic direction were already subtracted, remaining, a total of 188 modes. All the modes are Raman active, whereas only 141 are IR active (i.e. those with B_1, B_2 and B_3 symmetries). Table 1 summarizes the whole set of calculated modes together with their computed TMV directions and IR intensity. The latter values are expressed as the percentage of the maximum value equal to 107.4 km/mol obtained for the ω = 698 cm^{-1} and are employed to obtain a graphical representation of the IR computed spectrum as shown in Figure 4. The comparison between experimental and computed spectra is satisfactory, being particularly good in the 1600-500 cm^{-1} spectral region. At higher wavenumbers (i.e. ω > 2900 cm^{-1}), the agreement is less satisfactory due mainly to: (i) the anharmonic character of the CH stretching that dominates that part of the spectrum, (ii) the presence of overtones and combinations in the experimental data (which are not reproduced in the simulation) and (iii) the Fermi mixing behavior of both the phenyl and the alkyl CH stretching with the HCC bending modes of the CH and CH_2 chain groups as thoroughly discussed in Ref. 49. Beside the CH stretching part of the spectrum, that is well-separated from the other modes, different spectral zones can be distinguished. To do that, each mode has been described in terms of internal coordinates (see Figure 6 and Table 2) and ring deformations (see Figure 7). Mode description is reported in the last column of Table 1.

Three main regions can be identified in the 1600-500 cm^{-1} range of the s(2/1)2 sPS vibrational spectrum as follows:

(i) The zone between 1600 and 1490 cm^{-1} is associated with modes belonging exclusively to the phenyl groups. They are basically combinations of the stretching of the C-C bonds of the aromatic

rings (T), the in-plane bending of the phenyl hydrogen atoms (σ) and the stretching of the C-C bonds between the phenyl groups and the alkyl chain (R).

(ii) The zone between 1460 and 1150 cm^{-1} is characterized by the presence of complex modes (about 60% of the total) formed by a mixing between phenyl and chain internal coordinates; thus, they are expected to be conformationally sensitive. Some examples are the modes associated with the frequencies computed at 1383 and 1364 cm^{-1}, which can be described as the HCC bending and the wagging of the chain CH and CH_2 groups (ρ, χ, ζ, γ) coupled with the HCC in-plane bending of the phenyl groups (σ) and two types of CC stretching; namely that of the chain C atoms (S) and that of the C atoms that link the chain to the phenyl groups (R). Even though the complexity of the modes present in this zone, that can be inferred from the afore-mentioned cases, the difficult task of describing them can be enormously simplified by a direct visualization of the atomic displacements involved in each mode through graphical animations (see the CRYSTAL web site[67]). This graphical tool was already successfully employed for the description of the complex modes present in the trans-planar conformation of sPS as reported in Ref. 49.

(iii) The zone below 1150 cm^{-1} is similar to the above-described one but with an additional contribution of the phenyl ring deformations (see Figure 7). Conformationally sensitive peaks (i.e. those formed by a mixing between phenyl and chain internal coordinates) are expected to be a characteristic of this part of the spectrum; however, it is possible to observe that a great number of pure chain and pure phenyl group modes are also present. The majority of pure phenyl group modes are the wagging and the torsion about the periodic direction of the phenyl groups (ψ and Ω), the HCC out-of-plane bending of the phenyl H atoms (μ) and different kinds of ring deformations. On the other hand, the main type of pure chain modes encountered in this part of the spectrum involve the HCC bending and the torsions of the CH and CH_2 groups (τ, δ, ρ, ω and ω′) and the CC stretching (S).

For complex polymer helices such as s(2/1)2 s-PS, the direct comparison between computed and experimental frequencies can be a difficult task because of the presence of many vibrational modes that are often superimposed. It is, therefore, essential to have a tool that allows an unambiguous comparison between computed frequencies and experimental peaks. In this respect, as we recently shown[51], a precise experimental evaluation of the TMV directions of almost all of the s(2/1)2 s-PS vibrational modes (see Section IIIA) offers such an additional tool. The direct comparison between experimental and calculated data based on frequency values, relative intensities and TMV directions is then reported in Table 3. An excellent agreement is observed between the two sets of data. It is worth noticing that, in agreement with experimental observations, IR peaks for which is not possible to determine their TMV direction are associated with triplets of quasi-degenerated calculated frequencies whose computed TMV directions are oriented in the x, y and z directions (i.e. one direction for each component of the triplet). For instance, the IR peaks observed at 1584, 1494, 1453 and 1154 cm^{-1} are assigned to the triplets of the frequencies computed at 1591, 1495, 1452 and 1152 cm^{-1}, respectively (see Table 3).

By considering that totally symmetric (A) Raman active modes are usually stronger than B modes, we also give in Table 3 an assignment of the experimental Raman peaks. The comparison between experimental and calculated frequencies is quite good, even if Raman activities would be necessary to confirm the one-to-one correspondence.

C. Additional considerations based on comparison between experimental and calculated spectra

The good agreement between calculated and experimental results (Figure 4 and Table 3) suggests some additional considerations, which contribute to identify and rationalize the occurrence of packing sensitive and crystal-field-split peaks.

The splitting of the RAMAN peak located at 1451 cm^{-1} into a well resolved doublet with maxima at 1451 and 1440 cm^{-1}, which has been observed only for samples exhibiting the helical s(2/1)2 conformation, can be easily rationalized on the basis of the vibrational analysis of Tables 1-3 and of the graphical animations of the CRYSTAL web site.[67] In fact, as also clearly established by solid-state NMR experiments,[29] for the s(2/1)2 helix, which is obtained by sequences of internal rotation angles TTG^+G^+ or G^-G^-TT, the methylene carbons are all chemically equivalent but geometrically not equivalent, since 50% are internal (4 and 8 in Figure 1, the two adjacent C-C bonds exhibit T conformation) and 50% are external (2 and 6 in Figure 1, the two adjacent C-C bonds exhibit G conformation) with respect to the helix. The animations of the web site and Figure 8 clearly show that the vibrational A modes at 1463 and 1456 cm^{-1} (or the probably less intense 1448 cm^{-1} B_2 mode) are associated essentially only with the bending of the external and internal methylene groups, respectively.

In summary, the comparison between experimental and calculated spectra clearly indicates that RAMAN peaks observed for the semicrystalline helical samples at 1451 and 1440 cm^{-1} correspond to bending of external and internal methylenes of the s(2/1)2 helix, respectively. It is very interesting the occurrence, for a same conformationally ordered polymer chain, of two well-separated vibrational peaks corresponding to methylene bendings.

Our analysis also shows that the amorphous peak at 1379 cm^{-1}, being split in two peaks for semicrystalline γ, δ and ε samples (inset of Figure 4), corresponds to a single normal mode calculated for the isolated-helix (at 1383 cm^{-1}, Table 3). This suggests that this peak splitting is not due to the regular conformation of the helices of the crystalline phase (as for the Raman 1451 cm^{-1} peak) but to some intermolecular interactions occurring in the crystalline phases.

Most of packing-sensitive peaks located in the spectral region 1000-500 cm^{-1} (e.g., those observed at 967, 934, 906, 608, 601, 548, 535 and 503 cm^{-1} for δ form samples and at 969, 932-933, 909, 610, 599-600, 550, 539, 508 and 501 cm^{-1} for γ and ε form samples) correspond to

vibrational modes (calculated at 969-950, 921, 902, 605, 594, 540, 530 and 498 cm^{-1}, see Table 3) that include a substantial contribution from the bending of aromatic hydrogen atoms (μ, see Table 2). This result is easy to rationalize since, as clearly pointed out by the crystalline structures of the δ form[11-14] and of the ε form,[16] these hydrogen atoms, being external to the helix experience the largest non-bonded interactions with neighboring chains.

IV. Conclusions

The vibrational spectra (IR and Raman) of γ, δ and ε crystalline phases of syndiotactic polystyrene (sPS), i.e. phases presenting the s(2/1)2 helical conformation, have been compared with vibrational frequencies as computed at the B3LYP/6-31G(d,p) level of theory for an infinite s(2/1)2 helix.

For most infrared peaks, the orientation of the transition moment vector (TMV) of the corresponding vibrational modes have been experimentally established. In particular, the comparison between IR spectra of s-PS films presenting different kinds of (axial and uniplanar) orientations of the crystalline phase has not only allowed us to distinguish between TMV parallel and perpendicular to the helical axis but also (for the first time for a polymer) to establish the direction of the vectors in the plane perpendicular to the helical axis (x and y in Figure 1). This information on TMV directions has facilitated and validated the performed vibrational analysis (Table 3).

Just as an example, the comparison between experimental and calculated TMV directions has allowed the precise attribution of the two Raman peaks located at 1451 and 1440 cm^{-1} observed for semicrystalline helical samples, is due to two different vibrational modes associated with bending of external and internal methylenes of the s(2/1)2 helix, respectively (Figure 8).

Experimental evaluation of the TMV directions associated with polymer infrared peaks (even when perpendicular to the chain axis) can be also afforded for other semicrystalline polymers, if their crystalline structure is known. In fact, the experimental approach described in the present paper, although facilitated for s-PS by the occurrence of films with three different kinds of uniplanar orientations, can be extended to other semicrystalline polymers, if they can be obtained as films exhibiting at least one uniplanar orientation with chains parallel to the film plane (as generally obtained, e.g., by biaxial stretching). [68-72]

In particular, the information on the TMV direction could be obtained by a comparison (analogous to the procedure described in Figure 3) between peak intensities of IR spectra for unoriented and uniplanar films. A combination of this information with calculated spectra for infinite chains can lead to full normal vibrational analyses for several semicrystalline polymers, also presenting complex conformations in the crystalline phase.

V. Acknowledgements

Work performed for Regione Piemonte in the frame of the research project “Innovative Materials for Hydrogen Storage”. Financial support of the ”Ministero dell’Istruzione, dell’Università e della Ricerca” of ”Regione Campania” (Legge 5 and Centro di Competenza per le Attività Produttive) is gratefully acknowledged. We thank Prof. Adriano Zecchina of University of Torino and Dr. Christophe Daniel and Dr. Giuseppe Milano of University of Salerno for useful discussions.

References and Notes

(1) Chatani, Y.; Inagaki, Y.; Shimane, Y.; Ijitsu, T.; Yukimori, H.; Shikuma, H. *Polymer* **1993**, *34*, 1620.

(2) Chatani, Y.; Inagaki, T.; Shimane, Y.; Shikuma, H. *Polymer* **1993**, *34*, 4841.

(3) De Rosa, C.; Rizzo, P.; Ruiz de Ballesteros, O.; Petraccone, B.; Guerra, G. *Polymer* **1999**, *40*, 2103.

(4) Tarallo, O.; Petraccone, V. *Macromol. Chem. Phys.* **2004**, *205*, 1351.

(5) Tarallo, O.; Petraccone, V. *Macromol. Chem. Phys.* **2005**, *206*, 672.

(6) Daniel, C.; Galdi, N.; Montefusco, T.; Guerra, G. *Chem. Mater.* **2007**, *19*, 3302.

(7) Petraccone, V.; Tarallo, O.; Venditto, V.; Guerra, G. *Macromolecules* **2005**, *38*, 6965.

(8) Tarallo, O.; Petraccone, V.; Venditto, V.; Guerra, G. *Polymer* **2006**, *47*, 2402.

(9) Malik, S.; Rochas, C.; Guenet, J. M. *Macromolecules* **2006**, *39*, 1000.

(10) Galdi, N.; Albunia, A. R.; Oliva, L.; Guerra, G. *Macromolecules* **2006**, *39*, 9171.

(11) De Rosa, C.; Guerra, G.; Petraccone, V.; Pirozzi, B. *Macromolecules* **1997**, *30*, 4147.

(12) Milano, G.; Venditto, V.; Guerra, G.; Cavallo, L.; Ciambelli, P.; Sannino, D. *Chem. Mater.* **2001**, *13*, 1506.

(13) Sivakumar, M.; Mahesh, K. P. O.; Yamamoto, Y.; Yoshimizu, H.; Tsujita, Y. *Journal of Polymer Science, Part B: Polymer Phys.* **2005**, *43*, 1873.

(14) Gowd, E. B.; Shibayama, N.; Tashiro, K. *Macromolecules* **2006**, *39*, 8412.

(15) Rizzo, P.; Daniel, C.; De Girolamo Del Mauro, A.; Guerra, G. *Chem. Mater.* **2007**, *19*, 3864.

(16) Rizzo, P.; Daniel, C.; De Girolamo Del Mauro, A.; Guerra, G. It. Pat. N.SA2006A22 Italy.

(17) Guerra, G.; Vitagliano, V. M.; De Rosa, C.; Petraccone, V.; Corradini, P. *Macromolecules* **1990**, *23*, 1539.

(18) Chatani, Y.; Shimane, Y.; Inoue, Y.; Inagaki, Y.; Ishioka, T.; Ijitsu, T.; Yukimori, H. *Polymer* **1992**, *33*, 488.

(19) Rizzo, P.; Albunia, A. R.; Guerra, G. *Polymer* **2005**, *46*, 9549.

(20) Rizzo, P.; D'Aniello, C.; De Girolamo Del Mauro, A.; Guerra, G. *Macromolecules* **2007**, *40*, 9470.

(21) De Rosa, C.; Guerra, G.; Petraccone, V.; Corradini, P. *Polym. J.* **1991**, *23*, 1435.

(22) Corradini, P.; De Rosa, C.; Guerra, G.; Napolitano, R.; Petraccone, V.; Pirozzi, B. *Eur. Polym. J.* **1994**, *30*, 1173.

(23) Cartier, L.; Okihara, T.; Lotz, B. *Macromolecules* **1998**, *31*, 3303.

(24) Chatani, Y.; Shimane, Y.; Ijitsu, T.; Yukinari, T. *Polymer* **1993**, *34*, 1625.

(25) De Rosa, C.; Rapacciuolo, M.; Guerra, G.; Petraccone, B.; Corradini, P. *Polymer* **1992**, *33*, 1423.

(26) Rizzo, P.; Lamberti, M.; Albunia, A. R.; Ruiz de Ballesteros, O.; Guerra, G. *Macromolecules* **2002**, *35*, 5854.

(27) Immirzi, A.; De Candia, F.; Iannelli, P.; Vittoria, V.; Zambelli, A. *Makromol. Chem. Rapid. Commun.* **1988**, *9*, 761.

(28) Kobayashi, M.; Nakaoti, T.; Ishihara, N. *Macromolecules* **1989**, *22*, 4377.

(29) Grassi, A.; Longo, P.; Guerra, G. *Makromol. Chem. Rapid. Commun.* **1989**, *10*, 687.

(30) Gomez, M. A.; Tonelli, A. E. *Macromolecules* **1990**, *23*, 3385.

(31) Niquist, R. A. *Appl. Spectrosc.* **1989**, *43*, 440.

(32) Reynolds, N. M.; Savage, J. D.; Hsu, S. L. *Macromolecules* **1989**, *22*, 2867.

(33) Guerra, G.; Musto, P.; Karasz, F. E.; MacKnight, W. J. *Makromol. Chem.* **1990**, *191*, 2111.
(34) Vittoria, V. *Polym. Commun.* **1990**, *31*, 263.
(35) Filho, A. R.; Vittoria, V. *Makromol. Chem. Rapid. Commun.* **1990**, *11*, 199.
(36) Kobayashi, M.; Nakaoti, T.; Ishihara, N. *Macromolecules* **1990**, *23*, 7836.
(37) Reynolds, N. M.; Stidham, H. D.; Hsu, S. L. *Macromolecules* **1991**, *24*, 3662.
(38) Nakaoki, T.; Kobayashi, M. J. *Mol. Struct.* **1991**, *242*, 315.
(39) Musto, P.; Tavone, S.; Guerra, G.; De Rosa, C. *J. Polym. Sci. Polym. Phys.* **1997**, *35*, 1055.
(40) Tashiro, K.; Ueno, Y.; Yoshioka, A.; Kobayashi, M. *Macromolecules* **2001**, *34*, 310.
(41) Gowd, E. B.; Nair, S. S.; Ramesh, C. *Macromolecules* **2002**, *35*, 8509.
(42) Yoshioka, A.; Tashiro, K. *Macromolecules* **2003**, *36*, 3001.
(43) Musto, P.; Rizzo, P.; Guerra, G. *Macromolecules* **2005**, *38*, 6079.
(44) Albunia, A. R.; Musto, P.; Guerra, G. *Polymer* **2006**, *47*, 234.
(45) Reynolds, N. M.; Hsu, S. L. *Macromolecules* **1990**, *23*, 3463.
(46) Niquist, R. A.; Leugers, C. L.; McLachlan, R. D.; Thrill, B. *Appl. Spectrosc.* **1992**, *46*, 981.
(47) Kellar, E. J. C.; Galiotis, C.; Andrews, E. H. *Macromolecules* **1996**, *29*, 3515.
(48) Kellar, E. J. C.; Evans, A. M.; Knowles, J.; Galiotis, C.; Andrews, E. H. *Macromolecules* **1997**, *30*, 2400.
(49) Torres, F. J.; Civalleri, B.; Pisani, C.; Musto, P.; Albunia, A. R.; Guerra, G. *J. Phys. Chem. B* **2007**, *111*, 6327.
(50) Rastogi, S.; Gupta, V. D. J. *Macromol. Sci.* **1994**, *B33*, 129.
(51) Albunia, A. R.; Rizzo, P.; Guerra, G.; Torres, F. J.; Civalleri, B.; Zicovich-Wilson, C. M. *Macromolecules* **2007**, *40*, 3895.
(52) Rizzo, P.; Albunia, A. R.; Milano, G.; Venditto, V.; Guerra, G.; Mensitieri, G.; Di Maio, L. *Macromol. Symp.* **2002**, *185*, 65.
(53) Rizzo, P.; Costabile, A.; Guerra, G. *Macromolecules* **2004**, *37*, 3071.
(54) Rizzo, P.; Della Guardia, S.; Guerra, G. *Macromolecules* **2004**, *37*, 8043.
(55) Rizzo, P.; Spatola, A.; De Girolamo Del Mauro, A.; Guerra, G. *Macromolecules* **2005**, *38*, 10089.
(56) Albunia, A. R.; Rizzo, P.; Tarallo, O.; Petraccone, V.; Guerra, G. *Macromolecules*, **2008**, *41*, 8632
(57) Albunia, A. R.; Annunziata, L.; Guerra, G. *Macromolecules* **2008**, *41*, 2683.
(58) De Candia, F.; Filho, A. R.; Vittoria, V. *Makromol. Chem. Rapid. Commun.* **1991**, *12*, 295.
(59) Petraccone, V.; Auriemma, F.; Dal Poggetto, F.; De Rosa, C.; Guerra, G.; Corradini, P. *Makromol. Chem.* **1993**, *194*, 1335.
(60) Auriemma, F.; Petraccone, V.; Dal Poggetto, F.; De Rosa, C.; Guerra, G.; Manfredi, C.; Corradini, P. *Macromolecules* **1993**, *26*, 3772.
(61) Dovesi, R.; Saunders, V. R.; Roetti, C.; Orlando, R.; Zicovich-Wilson, C. M.; Pascale, F.; Civalleri, B.; Doll, K.; Harrison, N. M.; Bush, I. J.; D'Arco, P.; Llunell, M. *CRYSTAL06 user's manual*; Università di Torino: Torino, 2006.
(62) Becke, A. D. *J. Chem. Phys.* **1993**, *98*, 5648.
(63) Pascale, F.; Zicovich-Wilson, C. M.; Gejo, F. L.; Civalleri, B.; Orlando, R.; Dovesi, R. *J. Comp. Chem.* **2004**, *25*, 888.
(64) Civalleri, B.; D'Arco, P.; Orlando, R.; Saunders, V. R.; Dovesi, R. *Chem. Phys. Lett.* **2001**, *348*, 131.

(65) Zicovich-Wilson, C. M.; Pascale, F.; Roetti, C.; Saunders, V. R.; Orlando, R.; Dovesi, R. *J. Comp. Chem.* **2004**, *25*, 1873.

(66) Zicovich-Wilson, C. M.; Dovesi, R.; Saunders, V. R. *J. Chem. Phys.* **2001**, *115*, 9708.

(67) Zicovich-Wilson, C. M.; Bert, A.; Dovesi, R.; Saunders, V. R. *J. Chem. Phys.* **2002**, *116*, 1120.

(68) Heffelfinger, C. J.; Burton, R. L. *J. Polym. Sci.* **1960**, *47*, 289.

(69) Werner, E.; Janocha, S.; Hopper, M. J.; Mackenzie *Encyclopedia of Polymer Science and Engineering*, 2 ed.; Wiley Interscience: New York, 1986; Vol. 12.

(70) Gohil, R. M. *J.Appl.Polym.Sci.* **1993**, *48*, 1649.

(71) Uejo, H.; Hoshino, S. *J.Appl.Polym.Sci.* **1970**, *14*, 317.

(72) Rizzo, P.; Venditto, V.; Guerra, G.; Vecchione, A. *Macromol. Symp.* **2002**, *185*.

Figures

Figure 1: Along the chain axis (along z) representation of the s(2/1)2 helical chain of s-PS. Hydrogen atoms are not shown. The numbers indicate the sequence of the carbon atoms along the chain backbone. Symmetry considerations impose that TMV have to be parallel or perpendicular to the chain axis. TMV perpendicular to the chain axis have to be along the binary axes, indicated by x and y.

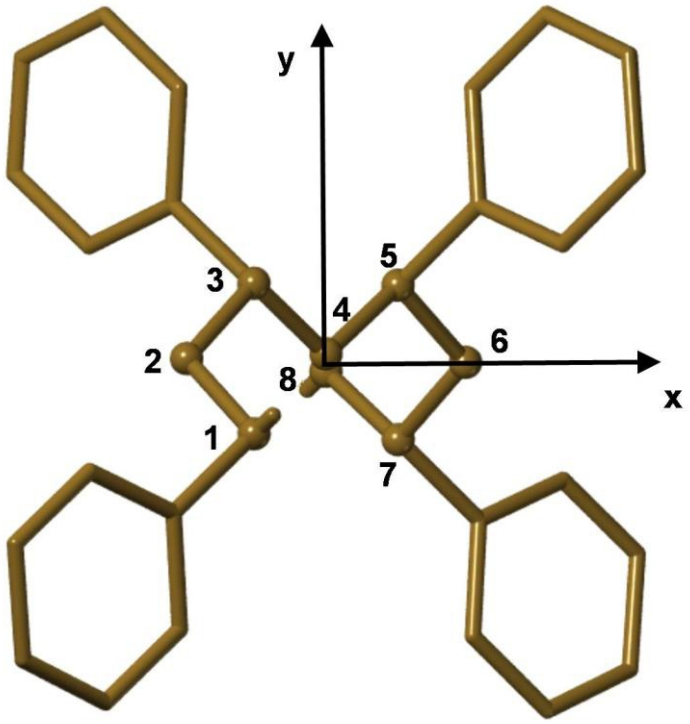

Figure 2: FTIR spectra taken with polarization plane parallel (thin lines) and perpendicular (thick lines) to the draw direction, for uniaxially oriented (for λ≈3) s-PS films including γ, δ and ε crystalline phases, after subtraction of amorphous phase contribution. The spectrum of a fully amorphous s-PS film is reported in (a). Peaks corresponding to vibrational modes being parallel (z) and perpendicular to the chain axis (⊥) have been indicated. (A) Wavenumber range 3150-400 cm^{-1} (B) Details of the spectral range 1100-820 cm^{-1}.

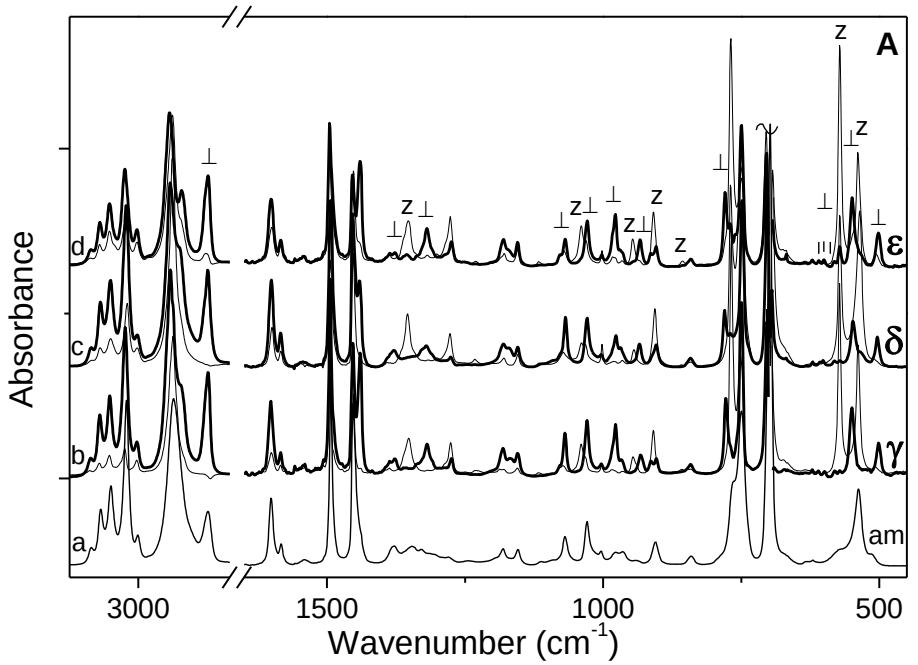

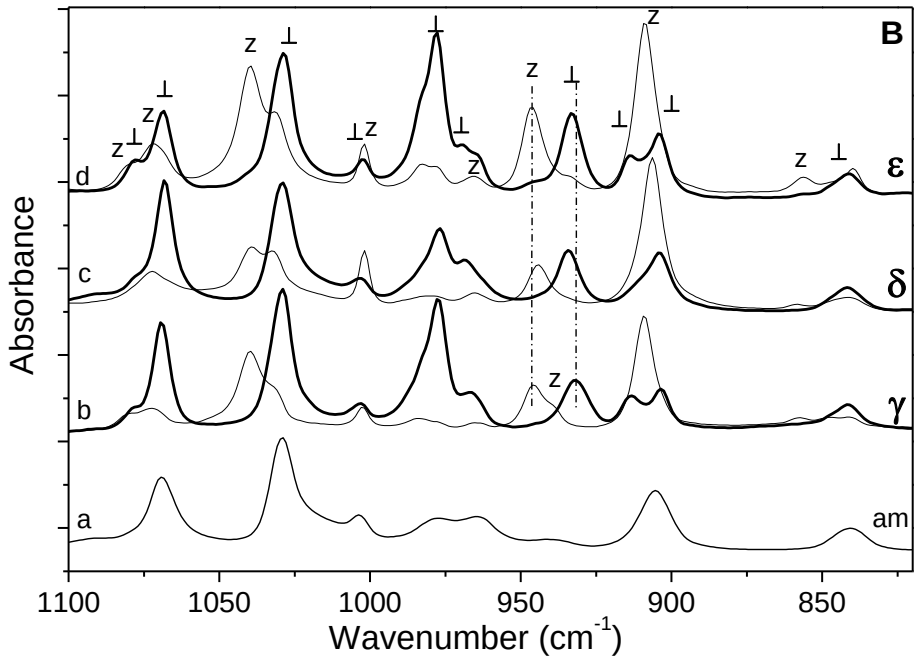

Figure 3: FTIR spectra of γ and δ form films with $a_{//}\,c_{//}$ (thin line) and $a_{\perp}\,c_{//}$ (thick line) uniplanar orientations. Peaks corresponding to vibrational modes parallel to the binary symmetry axes, being perpendicular to the chain axis, are labeled as x and y (see Figure 1). For the clarity of presentation, the labels x and y are indicated only for the spectra of δ and γ form films, respectively.

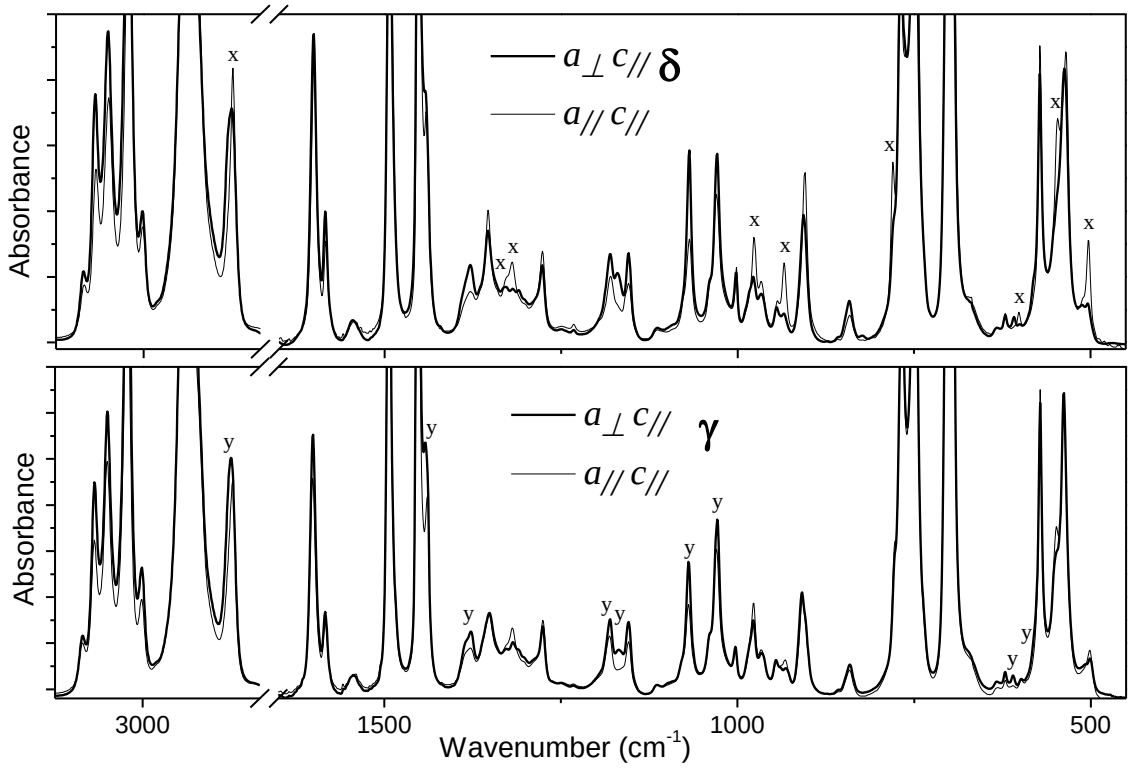

Figure 4: FTIR spectra of unoriented γ and δ form films of s-PS after subtraction of the spectrum of the amorphous phase compared with the *ab-initio* simulated spectrum of a s(2/1)2 helix of s-PS. Computed frequencies are scaled by 0.972. The inset figure allows visualization of the "amorphous" peak at 1379 cm^{-1}, its splitting in γ and δ semicrystalline phases and the calculated peak at 1383 cm^{-1}.

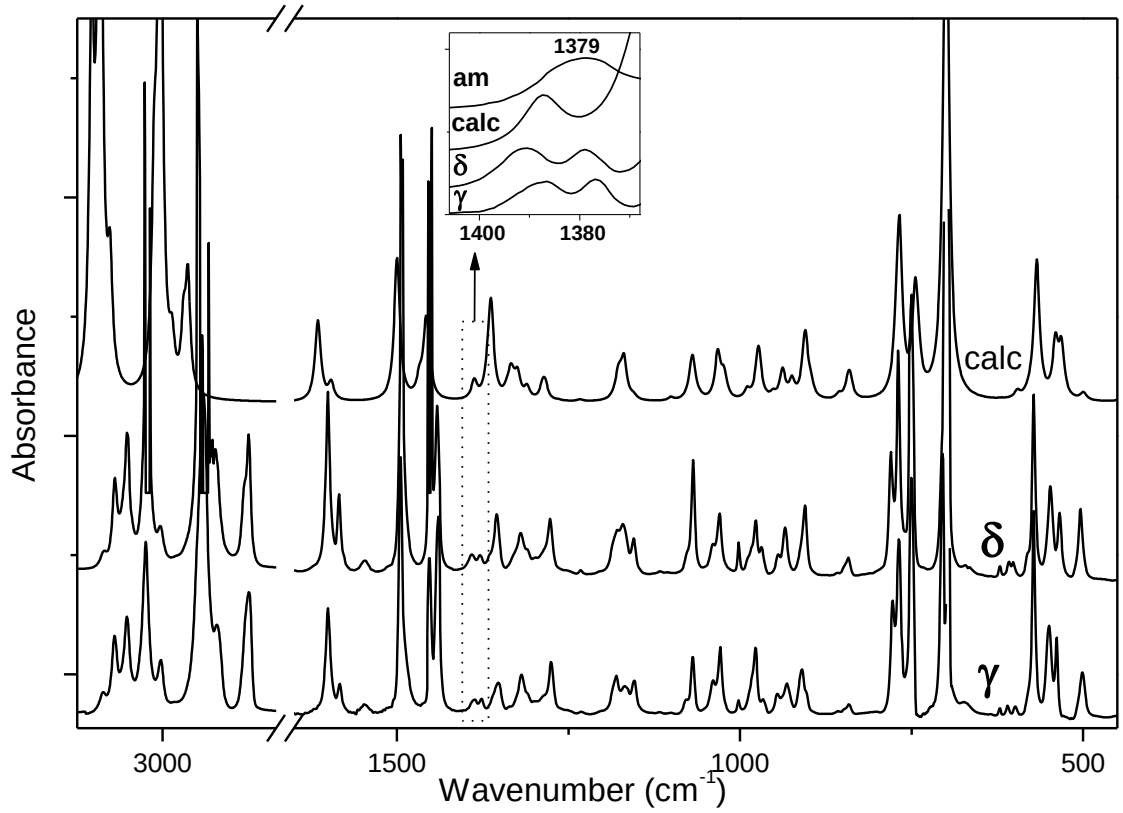

Figure 5: FT-Raman spectra in the wavenumber range 3700-100 cm^{-1}, of an amorphous s-PS films (trace A) and a semicrystalline film presenting the δ phase (trace B). The insets display a comparison between the amorphous spectrum (thin line) and the semicrystalline spectrum (thick line) in the wavenumber regions most sensitive to the presence of the crystalline phase.

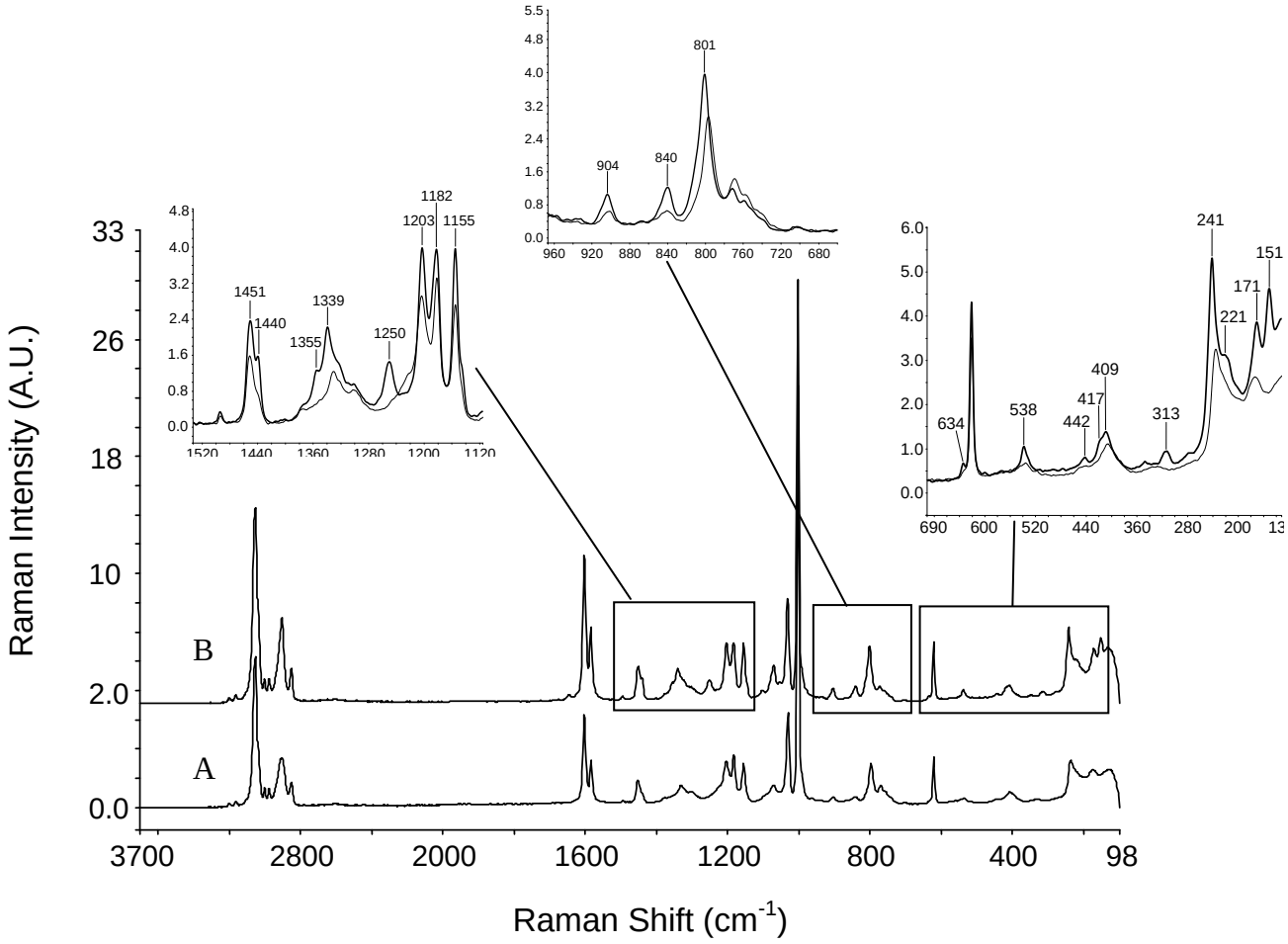

Figure 6: Schematic representation of the internal modes in a part of the s(2/1)2 infinite chain. Symbols are similar to those adopted in Ref. 49 for the normal vibrational analysis of the trans-planar conformation of sPS.

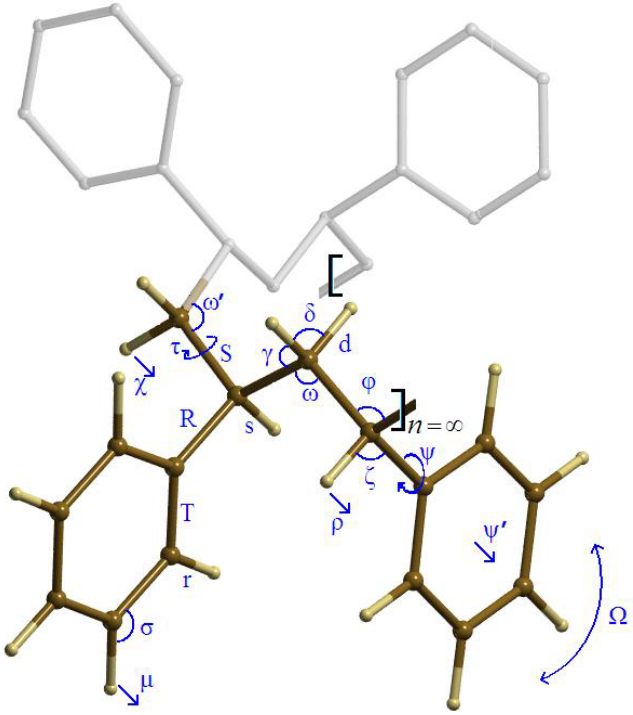

Figure 7: Schematic representation of the phenyl ring deformations associated with the modes in the zone below 1150 cm^{-1} of the calculated infra-red spectrum.

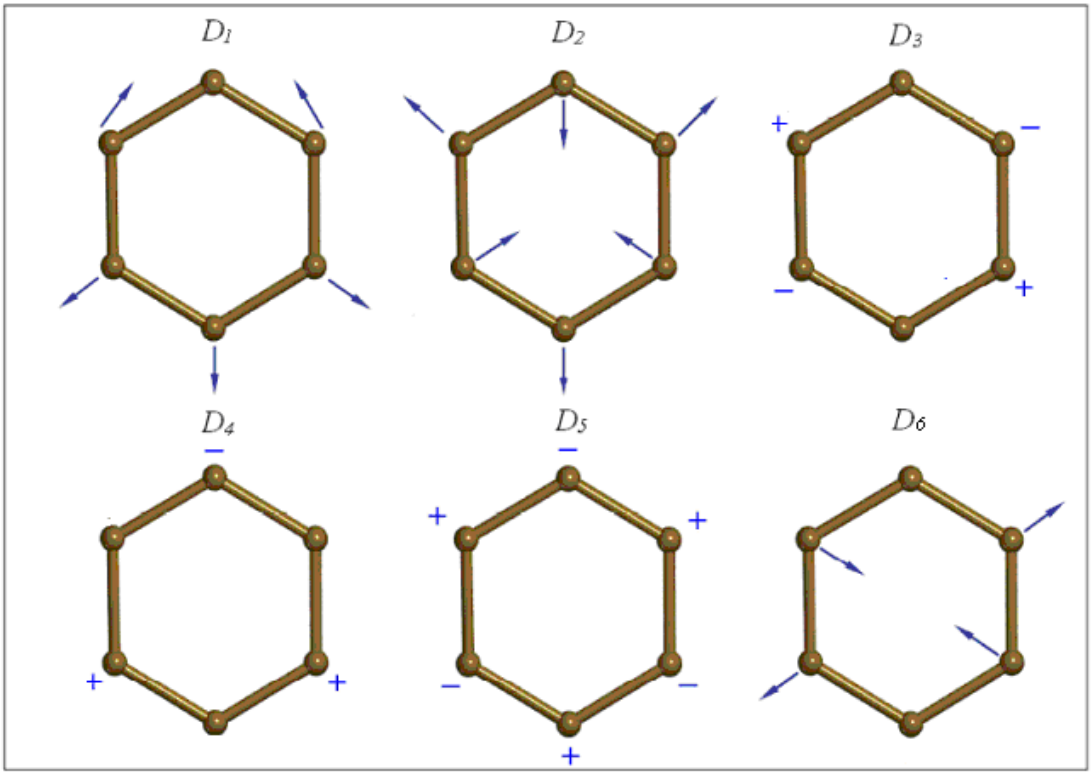

Figure 8: Along the chain axis (along z) representation of the s(2/1)2 helical chain of s-PS, showing the A (a) and A (b) vibrational modes calculated at 1456 and 1463 cm^{-1} and prevailingly assigned to the bending δ of internal and external methylenes, respectively. For the sake of clarity hydrogen atoms are shown only for the chain backbone.

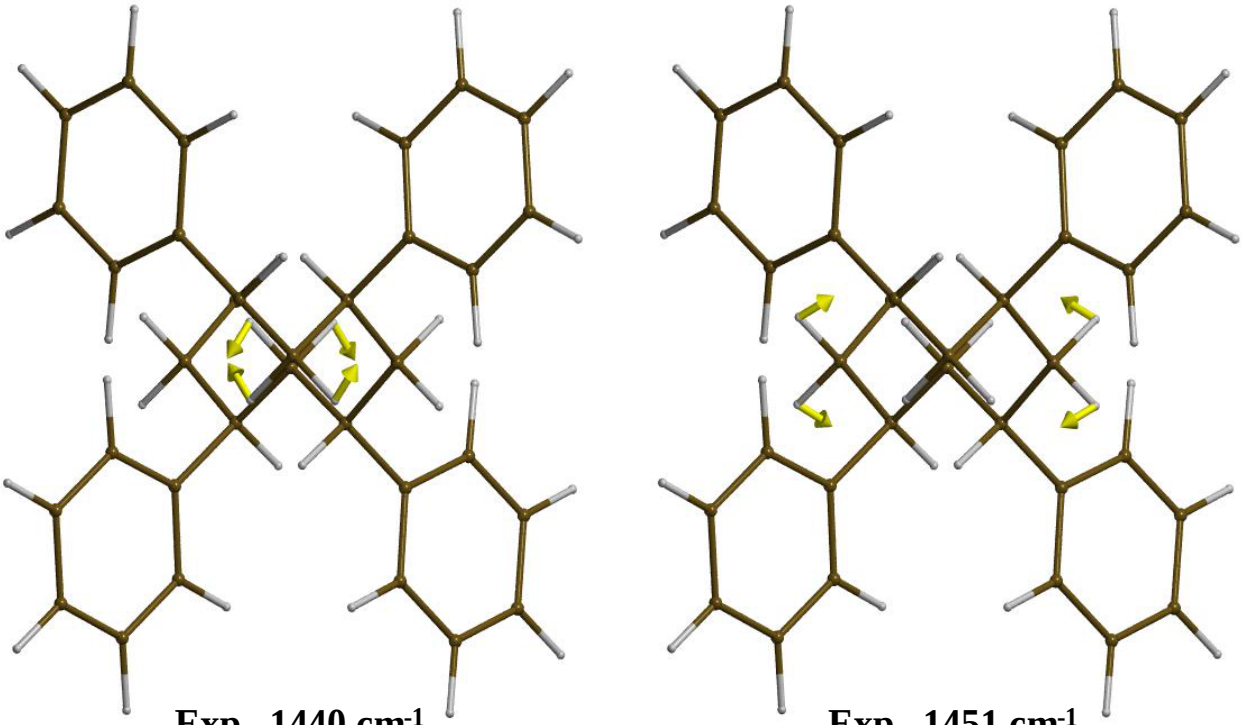

Exp. 1440 cm^{-1}
Calc. 1456 cm^{-1}
(a)

Exp. 1451 cm^{-1}
Calc. 1463 cm^{-1}
(b)

Tables

Table 1: The whole set of calculated normal modes. Reported frequencies (in cm^{-1}) are scaled by a factor equal to 0.972. The infrared intensities of each mode are expressed as percentage fraction of the maximum experimental intensity (ω = 698 cm^{-1}). The direction of the transition moment vector (TMV) for each mode is referred to the chain axis and defined in Figure 1. Normal mode symmetry refers to the *$P2_122$* rod group. Assignment is given in terms of internal coordinates as defined in Figures 6 and 7 and in Table 2. Normal modes shown as italic symbols have not been assigned to experimental peaks in Table 3.

ω	IR Intensity (%)	TMV Direction	Symmetry	Assignment
3115	151,1	x	B_3	r
3115	189,6	y	B_2	r
3115	73,3	z	B_1	r
3115	-	-	A	r
3103	-	-	A	r
3103	104,0	x	B_3	r
3102	188,5	y	B_2	r
3102	258,8	z	B_1	r
3098	-	-	A	r
3098	71,8	x	B_3	r
3096	151,3	y	B_2	r
3096	4,7	z	B_1	r
3088	-	-	A	r
3088	2,2	x	B_3	r
3088	4,2	y	B_2	r
3087	4,1	z	B_1	r
3084	-	-	A	r
3083	49,1	x	B_3	r
3082	27,8	y	B_2	r
3082	46,4	z	B_1	r
3005	204,1	x	B_3	d, s
2996	81,1	y	B_2	d, s
2995	508,7	z	B_1	d, s
2992	129,7	z	B_1	d, s
2984	-	-	A	s
2976	15,0	y	B_2	d, s
2973	35,0	x	B_3	d, s
2973	*2,0*	z	*B_1*	d, s
2956	-	-	A	d
2954	70,7	y	B_2	d, s
2947	-	-	A	d
2946	125,5	x	B_3	d
1612	-	-	A	T, σ
1611	18,6	x	B_3	T, σ
1610	24,1	y	B_2	T, σ
1610	51,6	z	B_1	T, σ
1591	-	-	A	T, σ

1591	3,2	x	B_3	T, σ
1591	13,8	y	B_2	T, σ
1591	2,2	z	B_1	T, σ
1496	-	-	A	R, T, σ
1496	56,0	x	B_3	R, T, σ
1495	58,4	z	B_1	R, T, σ
1495	48,8	y	B_2	R, T, σ
1463	-	-	A	δ
1463	19,3	x	B_3	δ
1456	-	-	A	δ
1454	35,5	y	B_2	T, σ, δ, ζ
1453	-	-	A	T, σ, δ, ζ
1452	5,6	x	B_3	T, σ, δ, ζ
1452	45,6	z	B_1	T, σ, δ, ζ
1448	16,2	y	B_2	δ, S
1383	21	y	B_2	γ, χ, ζ, σ, R, S
1364	13,3	z	B_1	ρ, χ, ζ, σ, R, S
1361	0,0	x	B_3	χ, ζ, R, S
1359	109,7	z	B_1	χ, ρ, S
1358	-	-	A	γ, ζ, R, S
1336	-	-	A	γ, ρ
1336	7,3	x	B_3	χ, ρ
1330	*6,8*	*y*	*B_2*	γ, χ, ρ
1329	20,2	x	B_3	γ, χ, ρ
1325	*6,2*	*z*	*B_1*	χ, ζ, σ
1324	*1,1*	*z*	*B_2*	T, σ
1324	-	-	A	T, σ, ζ
1320	*4,3*	*z*	*B_1*	σ, χ
1320	22,1	x	B_3	χ, γ, ρ, σ
1308	-	-	A	γ, R
1306	13,2	y	B_2	γ, ρ
1284	13,4	z	B_1	χ, ρ, R
1280	17	x	B_3	T, ζ, γ, σ
1260	*0,9*	*y*	*B_2*	χ, γ, ρ
1245	-	-	A	γ, ρ, R
1230	1,9	z	B_1	χ, ζ
1200	-	-	A	γ, ζ, σ, R
1189	*0,1*	*y*	*B_2*	ζ, σ, R
1183	*0,3*	*x*	*B_3*	ζ, σ, R
1179	*2,2*	*z*	*B_1*	ζ, σ, R
1179	-	-	A	σ, R
1178	*1,1*	*z*	*B_3*	σ, R
1174	13,3	y	B_2	σ
1173	10,4	z	B_1	σ
1170	*8,1*	*x*	*B_3*	γ, ρ, σ
1165	43,5	y	B_2	γ, ζ, σ
1153	-	-	A	σ

1153	0,0	x	B_3	σ
1152	0,5	y	B_2	σ
1152	4	z	B_1	σ
1139	-	-	A	γ, ρ, R, *D1*
1097	3,8	z	B_1	σ, τ
1091	*0,1*	*y*	*B_2*	ω, φ
1077	1,1	x	B_3	σ, *D1*
1076	-	-	A	σ, *D1*
1067	32,5	y	B_2	σ, *D1*
1064	23,0	z	B_1	σ, τ
1054	*2,0*	*x*	*B_3*	S
1038	-	-	A	S
1029	29,8	z	B_1	σ, *D1*
1029	14,5	x	B_3	T, σ, *D1*
1029	7,9	y	B_2	T, σ, *D1*
1028	-	-	A	T, σ. *D1*
1021	19,9	z	B_1	τ, φ
1018	8,2	y	B_2	γ, ρ
987	4,2	x	B_3	*D2*
986	5	z	B_1	*D2*
986	-	-	A	*D2*
986	1,2	y	B_2	*D2*
973	3,7	x	B_3	μ, τ
973	-	-	A	μ
970	52,2	x	B_3	μ, τ
969	0,9	y	B_2	μ, *D4*
969	4,9	z	B_1	μ, *D4*
955	-	-	A	μ, *D4*
953	*0,0*	*x*	*B_3*	μ, *D4*
950	0,9	y	B_2	μ, *D4*
948	4,8	z	B_1	μ, *D4*
943	-	-	A	ω, φ, *D2*
935	32,3	z	B_1	τ, *D2*
921	19,8	x	B_3	μ, τ, *D2*
905	8,6	y	B_2	μ
904	-	-	A	μ, *D5*
902	68,4	z	B_1	μ, *D5*
894	13,4	x	B_3	μ, *D5*, ω, φ
853	5,6	z	B_1	τ
845	-	-	A	μ
842	6,7	y	B_2	μ
841	0,2	x	B_3	μ
838	27,4	z	B_1	μ, *D1*
835	2,4	y	B_2	τ, ω, φ
795	-	-	A	R, γ
773	*3,5*	*y*	*B_2*	μ, *D6*
769	47,9	x	B_3	τ, μ, ρ, *D3*

765	172,2	z	B_1	μ, *D5*
755	-	-	A	μ, *D6*
742	100,0	x	B_3	τ, μ, ρ
740	*3,3*	*y*	*B_2*	τ, ρ, *D3*
739	35,3	z	B_1	τ, *D3*
703	-	-	A	μ, *D6*
700	*2,3*	*y*	*B_2*	μ, *D6*
699	169,4	x	B_3	μ, *D6*
697	468,7	z	B_1	μ, *D6*
626	-	-	A	*D3*
618	0,2	x	B_3	*D3*
617	*0,0*	*y*	*B_2*	*D3*
617	-	-	A	*D3*
617	0,4	z	B_1	*D3*
605	0,0	y	B_2	μ, *D3*
594	7,6	x	B_3	τ, μ, *D3*
577	4,9	y	B_2	τ, μ, *D3*
566	156,8	z	B_1	τ, μ, *D3*
540	60,0	x	B_3	τ, μ, *D4*
531	-	-	A	μ, *D4*
530	56,4	z	B_1	τ, μ, *D4*
500	3,8	z	B_1	τ
498	5,1	x	B_3	τ, μ, *D4*
444	*4,5*	*y*	*B_2*	μ, *D4*
433	-	-	*A*	ω, φ, *D4*, ρ
413	-	-	*A*	μ, *D4*
412	*0,3*	*y*	*B_2*	μ, *D4*
411	*0,3*	*x*	*B_3*	μ, *D4*
408	*1,8*	*z*	*B_1*	μ, *D4*
406	-	-	*A*	Ω, ω′
405	*0,1*	*y*	*B_2*	ω, *D4*
337	*4,7*	*z*	*B_1*	μ, *D4*, τ
297	*1,1*	*x*	*B_3*	ω′, *D5*
272	*0,6*	*z*	*B_1*	τ, Ω
256	*2,4*	*y*	*B_2*	τ, Ω
236	-	-	*A*	μ, *D5*, Ω
232	*2,2*	*x*	*B_3*	τ, Ω
223	*3,7*	*z*	*B_1*	τ, Ω
209	*0,5*	*x*	*B_3*	Ω ***
203	*0,9*	*x*	*B_3*	τ, μ, ρ
193	*0,2*	*y*	*B_2*	τ, *D5*
161	*0,0*	*y*	*B_2*	τ, Ω
158	-	-	*A*	Ω ***
140	-	-	*A*	Ω, ω
122	*1,6*	*z*	*B_1*	τ, *D5*
89	*0,0*	*z*	*B_1*	τ, χ, Ω
75	-	-	*A*	ψ

61	*0,2*	*x*	B_3	ψ
61	*0,2*	*y*	B_2	ψ
44	*0,0*	*x*	B_3	ψ′
42	*0,0*	-	*A*	ψ′
42	*0,1*	*y*	B_2	ψ′
37	*0,4*	*z*	B_1	τ, ψ
28	*0,1*	*y*	B_2	Ω
28	*0,4*	*z*	B_1	ψ′, CH_2 rot
26	-	-	*A*	Ω, CH_2 rot
19	*0,0*	*x*	B_3	ψ′, CH_2 rot

Table 2: Description of the internal coordinates shown in Figure 6 and employed for the mode assignment reported in Table 1. The superscripts *ph* and *ch* are used to discriminate atoms belonging to the phenyl groups and the chain, respectively.

Internal Coordinate	Description
d	stretching C^{ch}-H^{ch}
s	stretching C^{ch}-H^{ch}
r	stretching C^{ph}-H^{ph}
S	stretching C^{ch}-C^{ch}
R	stretching C^{ch}-C^{ph}
T	stretching C^{ph}-C^{ph}
δ	bending H^{ch}-C^{ch}-H^{ch}
γ	bending H^{ch}-C^{ch}-C^{ch}
ζ	bending H^{ch}-C^{ch}-C^{ph}
σ	bending H^{ph}-C^{ph}-C^{ph}
ω	bending C^{ch}-C^{ch}-C^{ch} internal methylene (y axes)
ω′	bending C^{ch}-C^{ch}-C^{ch} external methylene (x axes)
φ	bending C^{ch}-C^{ch}-C^{ch}
τ	torsion CH_2 group
ψ	torsion Phenyl group
ρ	H^{ch} wagging along the periodic direction (for CH)
χ	H^{ch} wagging along the periodic direction (for CH_2)
ψ′	Phenyl group wagging along the periodic direction
Ω	Backbone torsion along the periodic direction
μ	H^{ph} out of the plane

Table 3. Comparison between observed IR and Raman peak positions (ν_{exp}) for the amorphous phase and γ, δ and ε crystalline forms of sPS and calculated frequencies for a s(2/1)2 sPS infinite helix (ω_{calc}). Bold characters are used for peaks for which the attribution has been clearly validated by equal calculated and experimentally observed TMV directions.

Experimental		Calc.	Experimental				Calculated		
Raman			IR						
ν_{exp} [a]	I	ω_{calc} [a,b]	am γ ε	ν_{exp} [a] δ	TMV expt	I (δ)	ω_{calc} [a]	TMV calc	I
3106	w	3115 3103	3104		xyz	3	3115 3115 3115	x y z	151 190 73
		3098 3088 3084	3084		xyz	23	3103 3102 3102	x y z	104 189 259
3063 3054	sh s		3066		xyz	27	3098 3096 3096	x y z	72 151 5
3037	m		3031		xyz	40	3088 3088 3087	x y z	2 4 4
			3025		xyz	38	3083 3082 3082	x y z	49 28 46
3001	w		3002		zy	8			
2976	w	2984					3005	x	204
2936 2920	sh sh	2956 2947	2923	2930 2927	xyz	61 80	2996 2995 2992	y z z	81 509 130
2905	m			2907	xy	22	2976 2973	y x	15 35
				2857	**y**	21	**2954**	**y**	71
2850	w		**2848**		**x**	29	**2946**	**x**	126
1645	vw(cr) s		1600	**1604**	**z**	5	**1610**	**z**	52
1601		1612		1601 1600	xy	38	1611 1610	x y	19 24
1583	m	1591	1584		xyz	22	1591 1591 1591	x y z	3 14 2
1494	vw	1496	1494		xyz	91	1496 1495 1495	x y z	56 49 58

1451	m	1463	1453				xyz	86	1463 1453 1452 1452	x y z x	19 36 46 6
1440	m	1453	**1440**				**y**	33	**1448**	**y**	16
1373	vw		1379	1387 1376	1392 1378	1387 1376	yz y	4 3	1383	y	21
			1364				**z**	4	**1364**	**z**	13
1355	w (cr)	1358	1346	**1352**	**1354**	**1352**	**z**	16	**1359**	**z**	110
1339 1330	m (cr) w	1336	**1329**				**x**	3	**1336** **1329**	**x** **x**	7 20
1320	sh	1324	-	**1320**			**x**	10	**1320**	**x**	22
			1310				**y**	4	**1306**	**y**	13
1300	w	1308	1300				z	3	1284	z	13
1250	w (cr)	1245	1280	1277			z	11			
				1274	**1276**	**1274**	**x**		**1280**	**x**	17
1203	m	1200	1196	**1232**			**z**	1	**1230**	**z**	2
				1186			**y**	4	**1174**	**y**	13
1182	m	1179	1180				zy	4	1173	z	10
			-	**1167**	**1169**		**y**	13	**1165**	**y**	44
1155	m	1153 1139	1154				xyz	9	1153 1152 1152	x y z	0 0.5 4
			1112	**1117**			**z**	1	**1097**	**z**	4
			1069	**1078**			**x**	4	**1077**	**x**	1
1071	m	1076		**1069**			**y**	28	**1067**	**y**	33
1080	sh			**1080** **1071**			**z** **z**	5	**1064**	**z**	23
1052	vw		1029	**1040** **1032**			**z** **z**	7	**1029**	**z**	30
1031	m	1038		**1032**			**x**	14	**1029**	**x**	15
		1028		**1029**			**y**		**1029**	**y**	79
1002	vs		1004	1003			xy	8	1018 987	y x	8 4
				1002			**z**		**1021**	**z**	20
990	w	986	-	987			yz	1	986	z	5
			982					3	986	y	1.2
			977				**x**	15	**973** **970**	**x** **x**	4 52
			-	969	967	969	xy	6	950 969	x y	0.9 0.9
			965				**z**	1	**969** **948**	**z** **z**	5 5
			940	**946** **939**	**944**	**946**	**z**	5	**935**	**z**	32
				932	**934**	**933**	**x**	13	**921**	**x**	20
904	w	904	905	**914**			**y**	5	**905**	**y**	9

				909	**906**	**909**	**z**	13	**902**	**z**	68
				904			**x**	3	**894**	**x**	13
			-	**858**		**856**	**z**	1	**853**	**z**	6
			-	**847**			**y**	1	**842**	**y**	7
843	w	845	841				xyz	4	841 838 835	x z y	0.2 27 2
801	m	795									
771	vw	755	764	**778**	**780**		**x**	27	**769**	**x**	48
				769			**z**	57	**765**	**z**	172
758	vw		750	**750**			**x**	100	**742**	**x**	100
				754			**z**		**739**	**z**	35
702	vw	703	698				xz	>100	699 697	x z	169 469
638 621	w (cr) m	626	620 (621)				xz	3	618	x	0.2
		617							617	z	0.4
			-	**610**	**608**	**610**	**y**	4	**605**	**y**	0.0
			-	**599**	**601**	**600**	**x**	3	**594**	**x**	8
			581				**y**	2	**577**	**y**	5
			-	**572**			**z**	57	**566**	**z**	157
			-	**550**	**548**	**550**	**x**	24	**540**	**x**	60
538	w	531	539	**539**	**535**	**539**	**z**	15	**530**	**z**	56
			514	**508**	**510**	**508**	**z**	2	**500**	**z**	4
			-	**501**	**503**	**501**	**x**	21	**498**	**x**	5
442		433									
417		413									
409		406									
313		297									
241		236									
221		223									
171		158									
150		140									

[a] Data in cm^{-1}. [b] Raman vibrational frequencies refer to modes with *A* symmetry.
s = strong; m = medium; w = weak; sh = shoulder; v = very
cr = peak characteristic of the crystalline phase.